OPEN ACCESS

**Scholars International Journal of Chemistry and Material Sciences**

Abbreviated Key Title: Sch Int J Chem Mater Sci
ISSN 2616-8669 (Print) |ISSN 2617-6556 (Online)
Scholars Middle East Publishers, Dubai, United Arab Emirates
Journal homepage: http://saudijournals.com

**Original Research Article**

# Utilization of Zeolite-A/ZnO/Graphene Oxide Nanocomposite in the Adsorption Removal of some Heavy Metals from Pharmaceutical Wastewater

Ibrahim Salihu Zungeru[1], Muhammad Aliyu[1], Binta Saidu[1], Amos Ndarubu Tsado[1], John Tsado Mathew[2*], Olusayo Oyeronke Kolo[1], Rakiya Zubairu[1], Daniel Joseph[3], Bala Alhaji Suleman[3], Nathaniel Danazumi[4], Jibrin Yusuf Dabogi[1], Saheed Mustapha[5]

[1]Department of Biological Sciences, Niger State Polytechnic, PMB 01, Zungeru, Niger State, Nigeria.
[2]Department of Chemistry, Ibrahim Badamasi Babangida University Lapai, Niger state, Nigeria.
[3]Department of Physical Sciences, Niger State Polytechnic, PMB 01, Zungeru, Niger State, Nigeria.
[4]Department of Chemical Sciences, Federal Polytechnic, PMB 55, Bida, Niger State, Nigeria.
[5]Department of Chemistry, Federal University of Technology, PMB 65, Minna, Nigeria

**DOI:** https://doi.org/10.36348/sijcms.2025.v08i03.005 | **Received:** 28.04.2025 | **Accepted:** 03.06.2025 | **Published:** 14.06.2025

***Corresponding author:** John Tsado Mathew
Department of Chemistry, Ibrahim Badamasi Babangida University Lapai, Niger State, Nigeria

## Abstract

The synthesis and characterization of a novel zeolite-A/ZnO/graphene oxide (GO) nanocomposite were explored for the adsorption removal of heavy metals from pharmaceutical wastewater. The zeolite-A, ZnO nanoparticles, GO, and their composite were synthesized via hydrothermal, green, Hummer's, and wet impregnation methods, respectively. The synthesized samples were characterized using some analytical tools. X-ray diffraction analysis confirmed the successful synthesis of zeolite A, ZnO, and GO, with characteristic peaks aligning with standard crystallographic data. The composite structure displayed unique diffraction shifts, indicating the interaction between ZnO and the zeolitic framework. Scanning electron microscopy revealed distinct morphological features of individual components and their successful integration within the composite. Energy dispersive X-ray spectroscopy and elemental mapping further validated the composition of the nanocomposite and homogeneity. Brunauer–Emmett–Teller analysis demonstrated a high surface area of 115.70 $m^2/g$ for the composite, significantly higher than its individual constituents, alongside improved pore structure and volume. The adsorption performance was assessed for Cd, Fe, and Cr ions, showing superior removal efficiencies within 40–50 min, with maximum adsorption capacities of 107.92 mg/g (Cr), 98.28 mg/g (Fe), and 94.51 mg/g (Cd). Increased nanosorbent dosage and temperature positively influenced removal efficiency, achieving complete elimination at optimized conditions. Adsorption kinetics followed a pseudo-second-order model, confirming chemisorption as the dominant mechanism, while equilibrium data aligned with the Langmuir isotherm, indicating monolayer adsorption. The composite exhibited excellent stability and reusability across multiple cycles, demonstrating its potential for practical wastewater treatment applications and its sustainability for heavy metal remediation, offering a promising solution for mitigating environmental pollution from pharmaceutical wastewater.

**Keywords:** Wet impregnation, framework, surface area, reusability, remediation.



## 1. INTRODUCTION

Water pollution, especially heavy metal contamination, has become a priority environmental problem affecting human health and ecosystems for a long time. Heavy metals, due to their highly toxic and non-biodegradable nature, may persist in the environment, migrate, and accumulate in terrestrial and aquatic ecosystems for extended periods. In most cases, it is an ecological imbalance that metals like Pb, As, Hg, and Cr are greatly dangerous to chromium, especially as Cr(VI), a well-known carcinogenic agent, poses a danger to human beings and other forms of life even in low concentration (Etsuyankpa *et al*. 2024). Elimination of these harmful chemicals from wastewater streams is important in order to lessen their detrimental impact on human health and the ecological environment. Due to rapid industrial growth, the volume of generated pharmaceutical wastewater containing various organic and inorganic pollutants, including heavy metals, has increased notably (Razzak *et al*. 2024). Such pollutants often escape conventional processes of treatment due to

their complicated nature and toxicity. Thus, effective, economical, and environmentally friendly processes should be developed for their treatment.

Among the different methods of treatment like coagulation (Zahmatkesh *et al*. 2024), sedimentation (Raj *et al*. 2023), precipitation (Benalia *et al*. 2022), oxidation (Ponnusami *et al*. 2023), electrodialysis (Hu *et al*. 2023), and ion exchange (Guida *et al*. 2021), adsorption is one of the most studied techniques due to its simplicity, low cost, and the possibility of removing a wide category of pollutants, including heavy metals. Adsorption technology consists of the attachment of the contaminants onto the surfaces of the adsorbents, whose nature and performance strongly depend on the characteristics and properties of the adsorbents themselves (Bakhtiari *et al*. 2024). The development of novel and efficient adsorbents for heavy metal removal is, therefore, crucial to improving the overall effectiveness of adsorption-based treatment methods. Three nanoadsorbents that have been studied in wastewater treatment, especially for the removal of heavy metals, are zeolite-A, graphene oxide (GO), and zinc oxide (ZnO). These materials possess unique properties that make them especially suitable for adsorption applications. Such characteristics make zeolite-A, with its microporous framework, high surface area, and ion-exchange capacity, quite stable in structure and thus an excellent material for the removal of heavy metals from aqueous solution (Eren *et al*. 2024). GO is a two-dimensional carbon-based material containing a high surface area, a large number of oxygen-containing functional groups, and excellent mechanical properties, combining factors to provide a very high adsorption capacity for heavy metal ions (Mathew *et al*. 2024a). Besides, the photocatalytic properties of wide-bandgap semiconductor material ZnO are outstanding and can be further enhanced in its capability of pollutant absorption and destruction with high surface area upon UV light exposure (Abou Zeid and Leprince-Wang, 2024). Gopalakrishnan *et al*. 2015 investigated the effectiveness of graphene oxide nanosorbents in removing toxic heavy metal ions such as Pb(II), Ni(II), and Cr(VI) from pharmaceutical wastewater. The researchers found that GO completely removed chromium and lead ions from the effluent, while the removal efficiency of nickel ions increased with increasing concentrations of GO. A pH value of 8.0 with a minimum conductivity of 0.027 dS/m was obtained with 70 mg of GO in 100 mL of effluent for the optimum removal of all the heavy metal ions analyzed. Al-Abbad and Al Dwairi (2021) researched the efficiency of Jordanian natural zeolite for the removal of $Ni^{2+}$ ions from aqueous solutions. Their study focused on various factors that influenced the adsorption process, including contact time, initial metal concentration, adsorbent dosage, and temperature. The findings indicated that the maximum sorption capacity occurred at pH 4, with an adsorption capacity of 153.846 mg/g. Elsamra *et al*. (2024) investigated the adsorption performance of synthesized ZnO NPs for $Cd^{2+}$ and $Pb^{2+}$ ions. The optimum removal was achieved at pH 7, a contact time of about 20 min, and a sorbent dosage of 40 mg. The kinetic studies showed that the adsorption followed the pseudo-second-order kinetics, which meant that the rate-determining step involved chemisorption.

Although each of the individual materials mentioned above has excellent capability for heavy metal adsorption, their applicability within wastewater treatment systems can be minimal due to various issues linked with poor dispersion, agglomeration, and recyclability. In view of these limitations, creating nanocomposite materials that combine distinctive properties from different adsorbents has become a substantial interest. By incorporating zeolite-A, ZnO, and graphene oxide into a single nanocomposite, it possesses the advantage of each entity while enhancing adsorption performance because of such great synergy in various components, high stability, excellent recyclability, and effectiveness increase in removing heavy metals from wastewater. The combination of zeolite-A, ZnO, and graphene oxide can result in a highly efficient adsorbent for the removal of a broad range of heavy metals from pharmaceutical effluent. Structural features of zeolite-A, extensive surface area, and usefulness of graphene oxide, along with photocatalytic potential due to ZnO, can merge into a manifold effective solution against water purification difficulties. These components, upon integration into a composite matrix, may enhance separation ease, increase adsorption kinetics, and reduce the possibility for secondary contamination, hence making the composite material a very viable choice for real-world applications. Application of zeolite-A/ZnO/graphene oxide nanocomposite in heavy metals adsorption removal from pharmaceutical wastewater: a novel and promising technique. This is because the unique composition of the nanocomposite can provide better adsorption capacity, improved mechanical stability, and enhanced reusability compared with standard adsorbents. The following work is intended to value the effectiveness of zeolite-A/ZnO/graphene oxide nanocomposite in heavy metals removal, considering its efficiency in the effective removal of common pollutants such as Cr(VI), Fe(II), and Cd(II) ions, usually found in pharmaceutical wastewater.

## 2. MATERIALS AND METHODS

### 2.1 Materials and chemicals

The kaolin used in this work was obtained from a deposit in Paiko Local Government Area in Niger State, Minna, Nigeria. Potassium permanganate ($KMnO_4$, 99%), hydrochloric acid (HCl, 37%), and zinc acetate dihydrate ($Zn(CH_3COO)_2{\cdot}2H_2O$, 98%) were obtained from Sigma-Aldrich (USA). Sulphuric acid ($H_2SO_4$, 95-98%) and hydrogen peroxide ($H_2O_2$, 30%) were obtained from Merck (Germany) and used without further purification. Graphite powder (99.99%) was obtained from Alfa Aesar, UK, while sodium hydroxide (NaOH, 98%) was obtained from Xilong Chemicals,

Shanghai, China. Distilled water was prepared in the laboratory, Department of Chemistry, Ibrahim Badamasi Babangida University, Lapai, Niger State, Nigeria.

**2.2 Methods**

**2.2.1 Synthesis of zeolite-A**

Kaolin was calcined first in a muffle furnace at 800°C for 3 hr in order to change crystalline kaolin to amorphous metakaolin. The calcined metakaolin was kept at 500°C, and a 1 g sample was mixed with 10 $cm^3$ of NaOH solution of 3 $mol/dm^3$ and stirred on a magnetic stirrer for 2 hr. The obtained homogenous solution was transferred to the Teflon-lined stainless-steel autoclave for hydrothermal reaction at different temperatures ranging from 105 °C for 12 h at autogenous pressure and under static conditions. Afterward, the resultant obtained solid products, after the reactions, were filtered through the use of Whatman-42 filter paper, followed by sufficient washing in de-ionized water. Finally, the resultant solid products were dried overnight in a hot air oven to produce the final product, zeolite-A (Mathew *et al*. 2023a).

**2.2.2 Preparation of graphene oxide**

GO was prepared using Hummer's method. First, 50 $cm^3$ of concentrated (98.95%) $H_2SO_4$ is poured into a beaker and put in an ice bath to keep the temperature below 20°C. Then, 2 g of graphite powder is put into the solution while stirring at 500 rpm. $H_2SO_4$ is the oxidizing agent for graphite. Then, 6 g of $KMnO_4$ is added slowly to the reaction due to its exothermic nature. After a few minutes, the ice bath is removed and then stirred at 50 °C for 3 h. Then, the ice bath is refilled, and 200 cm3 of de-ionized water is added drop by drop to control the exothermic reaction. After 15 minutes, another 150 cm3 of de-ionized water is added. To quench the reaction, 10 $cm^3$ of $H_2O_2$ is slowly added. The color changes from dark brown to yellow. Undesirable extracts are removed by centrifugation at 4000 rpm. Then, it is washed with a 1:9 aqueous HCl solution to remove sulfate ions, followed by de-ionized water. Then, it is dried in a hot air oven at 60°C overnight, and graphene oxide GO powder is obtained (Mathew *et al*. 2023b).

**2.2.3 Green synthesis of ZnO nanoparticles**

The green synthesized ZnO nanoparticles were performed, as illustrated in Fig. 1. A 100 $cm^3$ solution of freshly prepared Guava leaf extract, consisting of water, was heated at 80°C. 10 g of zinc acetate was added to the solution and was continuously stirred using a magnetic stirrer for 4 hr until the reaction was complete. After stirring, the liquid was brought to a pH of 10 using NaOH and mixed for 10 minutes. The solution was washed with de-ionized water and filtered properly to avoid contamination. The crystalline resultant product was obtained after oven drying at 105 ºC of the solution and further calcination at 450 ºC in a muffle furnace for 3 h and characterized.

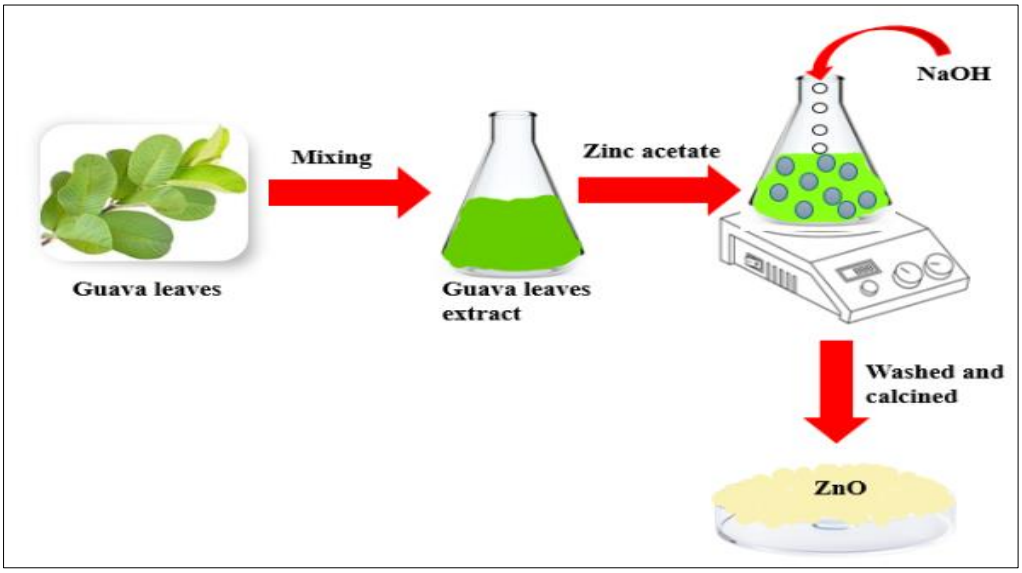


**Fig. 1: Green route for the synthesis of ZnO nanoparticles**

**2.2.4 Preparation of zeolite A-ZnO-GO nanocomposite**

In this work, the wet-impregnation method was used for the synthesis of zeolite A-ZnO-GO nanocomposites. First, 0.2 g of zeolite A was dispersed in 20 $cm^3$ de-ionized water under ultrasonication for 60 min. Later, ZnO nanoparticles (0.2 g) and GO (0.2 g) were added into the suspension under continuous ultrasonication for complete dispersion. This suspension was further stirred at 80 °C to allow the complete evaporation of water and was dried overnight at the same temperature. The prepared nanocomposite was termed zeolite A-ZnO-GO (Musa *et al*. 2024).

**2.2.5 Characterization of nanomaterials**

XRD was performed to investigate the crystallinity and phase composition of nanomaterials. Finally, the prepared nanocomposites of Zeolite-A-ZnO-GO were characterized by SEM, along with EDX

analysis, with the aim of investigating the surface shape, particle size, and elemental contents of the composites. The components present in the composites and their distribution were revealed by EDX analysis, while morphological features from SEM provided insight into the structural properties of the composite. After degassing the samples at 140 °C, the surface area analysis using the BET model was done using an apparatus, Belsorp-miniX, Germany, for the determination of the specific surface area of the adsorbents.

### 2.2.6 Batch adsorption studies

The specific aim of the conducted batch adsorption studies was to investigate the influence of contact time on the removal of Cr(VI), Fe(II), and Cd(II) from pharmaceutical wastewater. The exposure time ranged between 0-50 min. In each experiment, 0.1 g of the prepared adsorbent was added to 100 cm3 of wastewater in a 250 $cm^3$ conical flask. Removal efficiency was performed at different times of shaking in a rotary shaker at 120 rpm. The dose of adsorbent was varied between 0.3 and 0.8 g to understand its effect on the removal of metal ions. For each experiment, the appropriate amount of adsorbent was added to the flask filled with 100 $cm^3$ of wastewater. The rotary shaker was stirred at 120 rpm with a constant temperature of 20±1 °C. In different dosages, the removal of metal ions was determined. The temperature effect on adsorption was investigated by varying from 30°C to 70°C. A 250 $cm^3$ conical flask containing 0.1 g of the adsorbent was added to the 100 $cm^3$ solution of the metal ions. The flask was kept at 120 rpm of agitation and put in a temperature-controlled environment. The efficiency of the removal of metal ions was checked at different temperatures. The % removal of the metal ions was calculated by equation 1, and the adsorption capacity of the metal ions by equation 2 (Shaba *et al*. 2024)

$$\%\, removal = \frac{C_i - C_f}{C_i} \times 100 \qquad (1)$$

$$Adsorption\ capacity = \frac{C_i - C_f}{M} V \qquad (2)$$

where $C_i$ and $C_f$ are the initial and final concentrations of metal ions (mg/$dm^3$), $V$ is a known volume of wastewater ($cm^3$), and $M$ is a known mass of the adsorbent (g)

A number of cycles of adsorption-desorption were performed in order to analyze the recyclability of the adsorbent. The 0.01 M NaOH was used for 10 min to renew the metal ion-adsorbed sorbents. Then, the adsorbent was washed with de-ionized water until neutral pH and used again in subsequent cycles. After some cycles, the adsorption efficiency was followed in order to investigate the effectiveness of the adsorbent (Mathew *et al*. 2024b).

## 3. RESULTS AND DISCUSSION

### 3.1 Characterization

#### 3.1.1 XRD

Fig. 2 depicts the X-ray patterns of zeolite-A, ZnO, GO, and their composite. The successful synthesis of zeolite A and its crystalline nature was confirmed since the synthesized products matched the characteristic peaks of zeolite A at 2θ values of 7.2°, 10.3°, 12.6°, 16.2°, 21.8°, 24°, 26.2°, 27.2°, 30°, 30.9°, 31.1°, 32.6°, 33.4°, and 34.3°, as presented in Fig. 2. Fig. 2 shows the XRD pattern of ZnO. The spectra at diffraction lines (110), (002), (101), (102), (110), (103), (200), (112), (203), and (201), respectively, show diffraction peaks at 31.77°, 34.42°, 36.25°, 47.54°, 56.60°, 62.85°, 66.38°, 67.96°, 69.10°, and 89.61°. They are a = b = 3.25 Å for the cell constants. These values are indexed as the hexagonal zincite structure and agree with the peaks of the standard card file JCPDS-00-036-1451. The presence of these peaks indicates the successful synthesis and crystalline phase of ZnO. Fig. 2 depicts the XRD pattern of GO. It is observed from the figure that the oxidation of graphite introduces a peak at an angle of 11.5° corresponding to the (001) plane with an interlayer spacing of 7.7 Å. With this in view, the absence of any second strong peak suggests the complete oxidation of graphite to produce graphene oxide. It is also highly broad in nature, which reveals that the GO prepared has an exfoliated and disordered structure, as was expected with such an addition of functional groups containing oxygen. Fig. 2: XRD patterns of the ZnO and GO-incorporated zeolite A. The XRD patterns of pure zeolite A and zincite-structured ZnO crystals can be seen in the figure. Obviously, the XRD pattern of zeolite-A/ZnO/GO is different from the others, reflecting some structural changes in ZnO. The changes in relative peak intensities and slight shifts to higher diffraction angles indicate the compression of the crystallite structure of zeolite-A due to the crystal growth of ZnO nanoclusters. Such an effect represents the interaction between ZnO and the framework of the zeolite that may alter the characteristics and performance of the material for catalytic or adsorption applications.

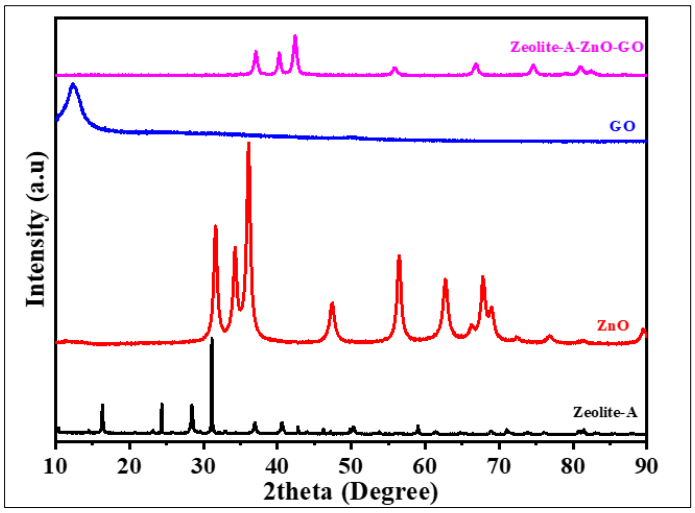


**Fig. 2: X-ray patterns of zeolite-A, ZnO, GO, and zeolite A-ZnO-GO nanocomposite**

### 3.1.2 SEM

As can be seen from the SEM micrographs, hydrothermal treatment of metakaolin in a concentration of NaOH led to the formation of zeolite A (Fig. 3a). Zeolitic products are clearly present with their typical platy morphology and hexagonal platy crystal outlines, suggesting the presence of kaolinite (Fig. 3a). Quartz, which could be observed in SEM pictures, was also confirmed by results obtained from EDX as depicted in Fig. 4(a). The morphology of ZnO nanoparticles was investigated using SEM analysis. From the micrograph in Fig. 3(b), it is observed that ZnO has a pseudo-spherical shape and trend toward particle-like morphology. ZnO particles also show significant agglomeration in the SEM image, which their high surface energy could justify along with relatively medium-specific surface area compared to zeolite-A. Due to these characteristics, the ZnO nanoparticles have a great tendency to be aggregated and eventually form larger clusters. The synthesized ZnO nanoparticles were confirmed by the EDX results, as presented in Fig. 4(b), indicating the non-presence of impurities. It can be seen that the surface of GO possesses stratified and wrinkled flakes in its SEM micrograph in Fig. 3(c). The presence of flakes indicates the formation of GO due to the oxidation of graphene layers. In Fig. 3(d), the GO structure is not visible in the SEM image of the synthesized composite. Instead, GO and ZnO are present on the zeolitic surface in the form of heterogeneously dispersed agglomerates. Similarly, the SEM image of the composite does not reveal the characteristic shape of zeolite A. However, the presence of this material was demonstrated in the composite by EDX (Fig. 4d) and elemental mapping (Fig. 5), thus ensuring successful incorporation.

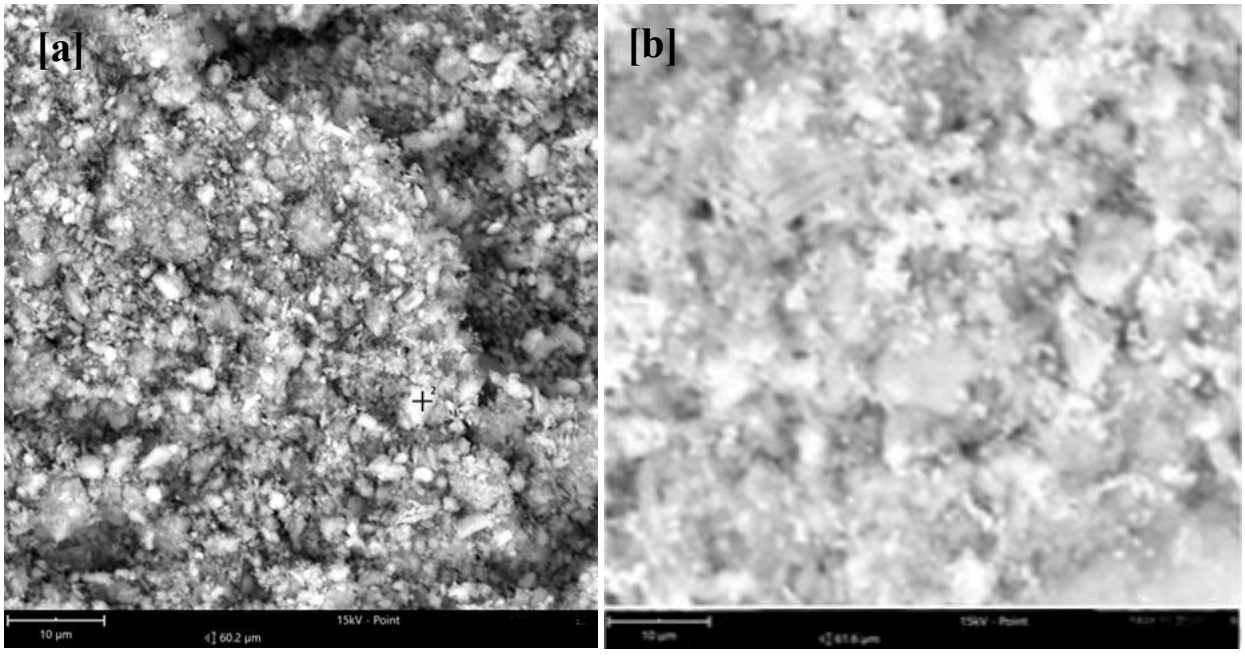

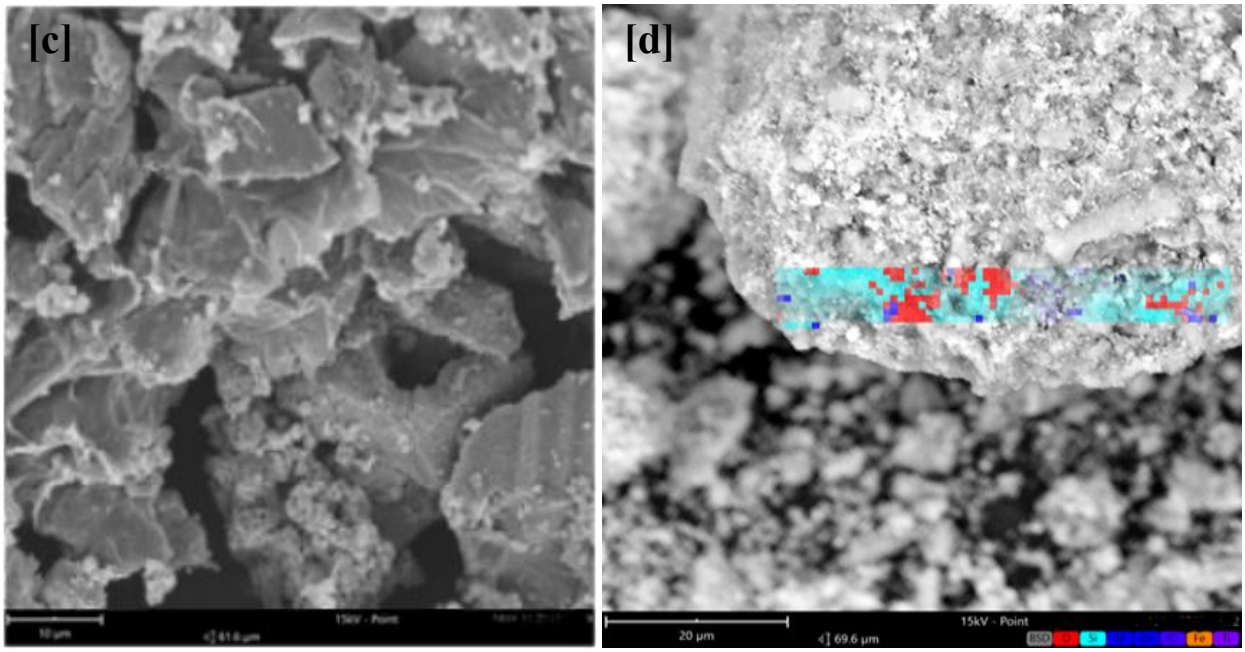


**Fig. 3: The SEM images of (a) zeolite-A (b) ZnO (c) GO and (d) zeolite A-ZnO-GO**

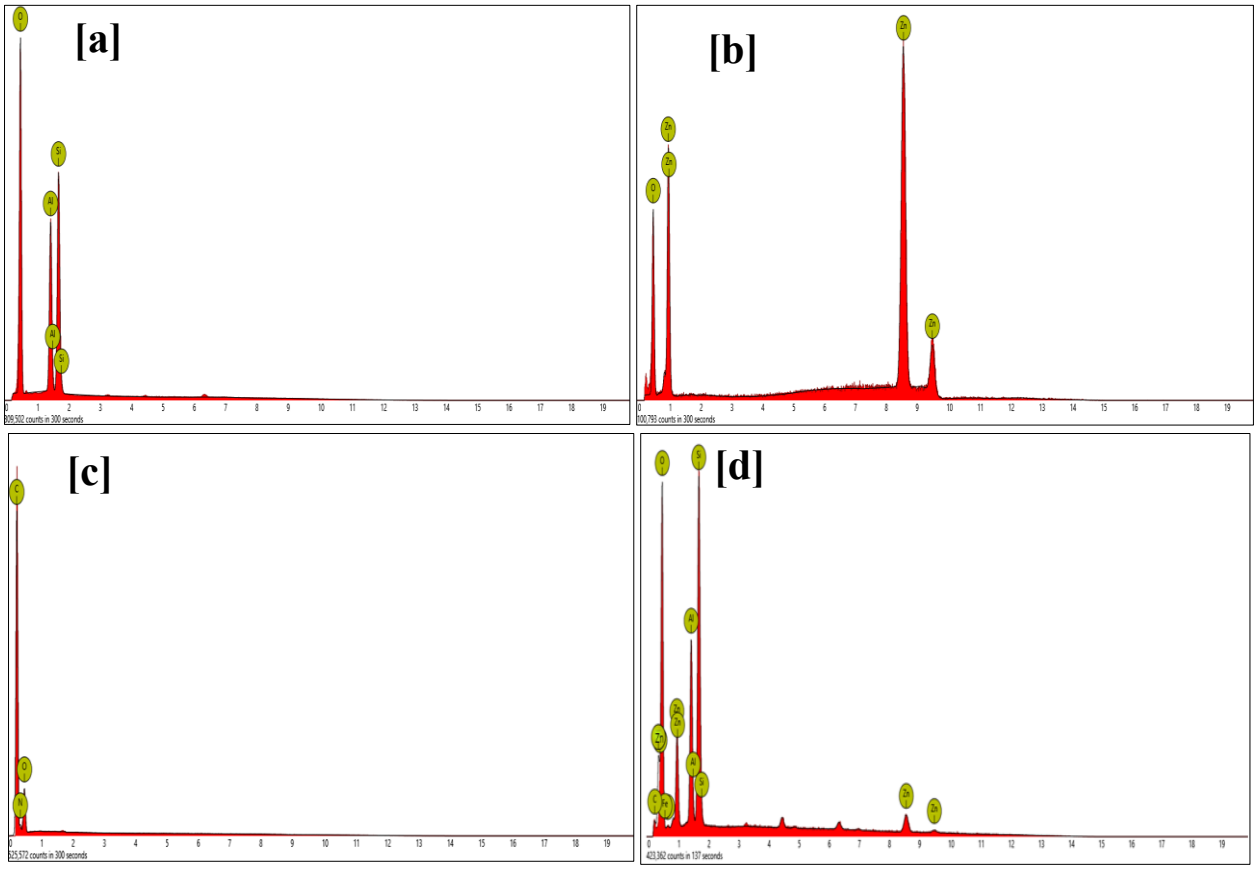


**Fig. 4: The EDX spectra of (a) zeolite-A (b) ZnO (c) GO and (d) zeolite A-ZnO-GO**

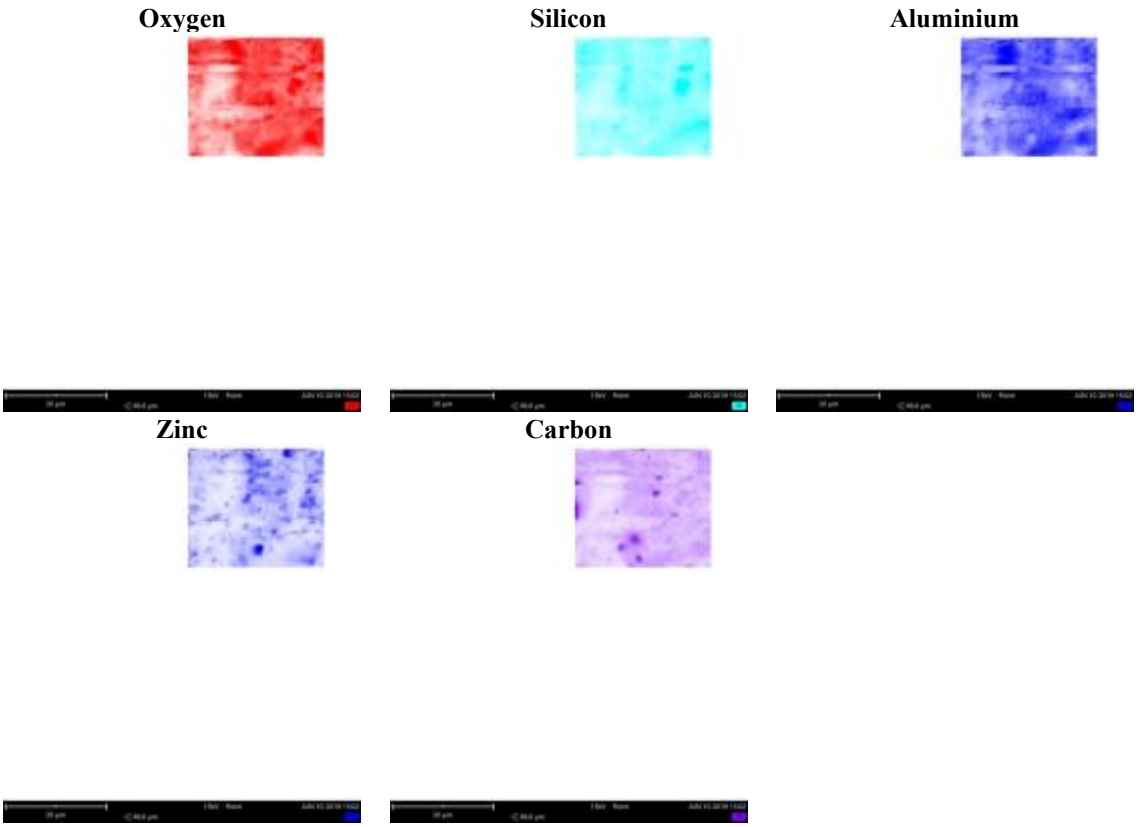


**Fig. 5: The EDX mapping of zeolite A-ZnO-GO nanocomposite**

### 3.1.3 BET

The BET data in Table 1 presents the surface area, pore size, and pore volume of the different adsorbents. Zeolite-A had a much smaller surface area of 17.35 $m^2/g$ compared to ZnO, which was 26.09 $m^2/g$, and GO, which was 62.54 $m^2/g$. This can be attributed to the crystalline nature and small external surface area of zeolites. Because of its layered structure and high porosity, the surface area of GO is the largest among all the constituent components and equals 62.54 $m^2/g$. The surface area of the composite zeolite-A/ZnO/GO was the largest, 115.70 $m^2/g$, showing evidence that the components had combined successfully and the total adsorption capacity was increased. Besides, the pore size of GO was 3.213 nm, whereas for Zeolite-A, it was 8.151 nm, followed by 5.076 nm for ZnO. The smaller pore diameter of the composite (2.842 nm) indicates that the integration of materials results in a more compact and ordered porous network, possibly because of interaction between the components, leading to a more compact adsorption surface with better accessibility. Pore volume increased for ZnO (0.2851 cc/g), GO (0.3712 cc/g), and Zeolite-A (0.2115 cc/g). Since the composite has the highest pore volume, 0.3965 cc/g, it can be said that the combination of the components increases porosity overall. In applications such as adsorption, this increased pore volume is definitely a positive feature since it provides more room within the material for the trapping of molecules.

**Table 1: Summary of BET results of zeolite-A, ZnO. GO and zeolite-A/ZnO/GO**

| Adsorbent | Surface area ($m^2/g$) | Pore size (nm) | Pore volume (cc/g) |
|---|---|---|---|
| Zeolite-A | 17.35 | 8.151 | 0.2115 |
| ZnO | 26.09 | 5.076 | 0.2851 |
| Graphene oxide | 62.54 | 3.213 | 0.3712 |
| Zeolite-A/ZnO/GO | 115.70 | 2.842 | 0.3965 |

## 3.2 Adsorption studies

### 3.2.1 Contact time

Fig. 6 shows the Cd, Fe, and Cr ions removal efficiency from pharmaceutical wastewater as a function of contact time for different adsorbents. For all the tested metal ions, the adsorption rate stabilized almost perfectly within 40-50 min and thus indicated the saturation of the active sites. Compared with the individual adsorbents, the zeolite A-ZnO-GO composite had superior adsorption capacity and the highest removal efficiencies. The removal percentage for Cr (Fig. 6a) rose in the first 40 min, reaching 70.11% for zeolite A-ZnO-GO and 47.1%, 57.07%, and 60.44% for zeolite-A, ZnO, and GO, respectively. The rates either hardly changed or were about the same after 50 min, indicating that the adsorption sites were saturated. These are attributed to

the varying nature of the adsorbent surface and their interaction with Cr ions. The maximum removal, 66.7%, was by zeolite A-ZnO-GO in 40 min, followed by GO, 63.07%; ZnO, 55.62%; and zeolite-A, 51.3% for the removal efficiency of Fe ions. It is noted that a similar trend is observed, where after 50 min, the margin of effectiveness decreased; this might indicate that the adsorption sites were nearly exhausted. These differences in pore structure, surface chemistry, and accessible functional groups for metal ion binding are responsible for the diversity in Fe removal.

In the case of Cd (Fig. 6c), the removal efficiency increased gradually in 40 min, having started rapidly. The maximum removal was by zeolite A-ZnO-GO (65.51%), followed by GO (62.51%), ZnO (58.04%), and zeolite-A (55.8%). Beyond 50 min, there was a slight decline in adsorption, showing that the system had reached a state of equilibrium and that longer times had little effect. The difference in the removal efficiencies of Cr, Fe, and Cd is due to their differing ionic properties and affinities to the adsorbent. The composite exhibited better adsorption performance due to the complementary nature of its constituents with increased surface area, more functional groups, and improved adsorption sites. Due to the presence of a large number of pores, an elevated surface charge, and the synergetic effect of nanoparticles, zeolite A-ZnO-GO is an efficient adsorbent in heavy metals removal.

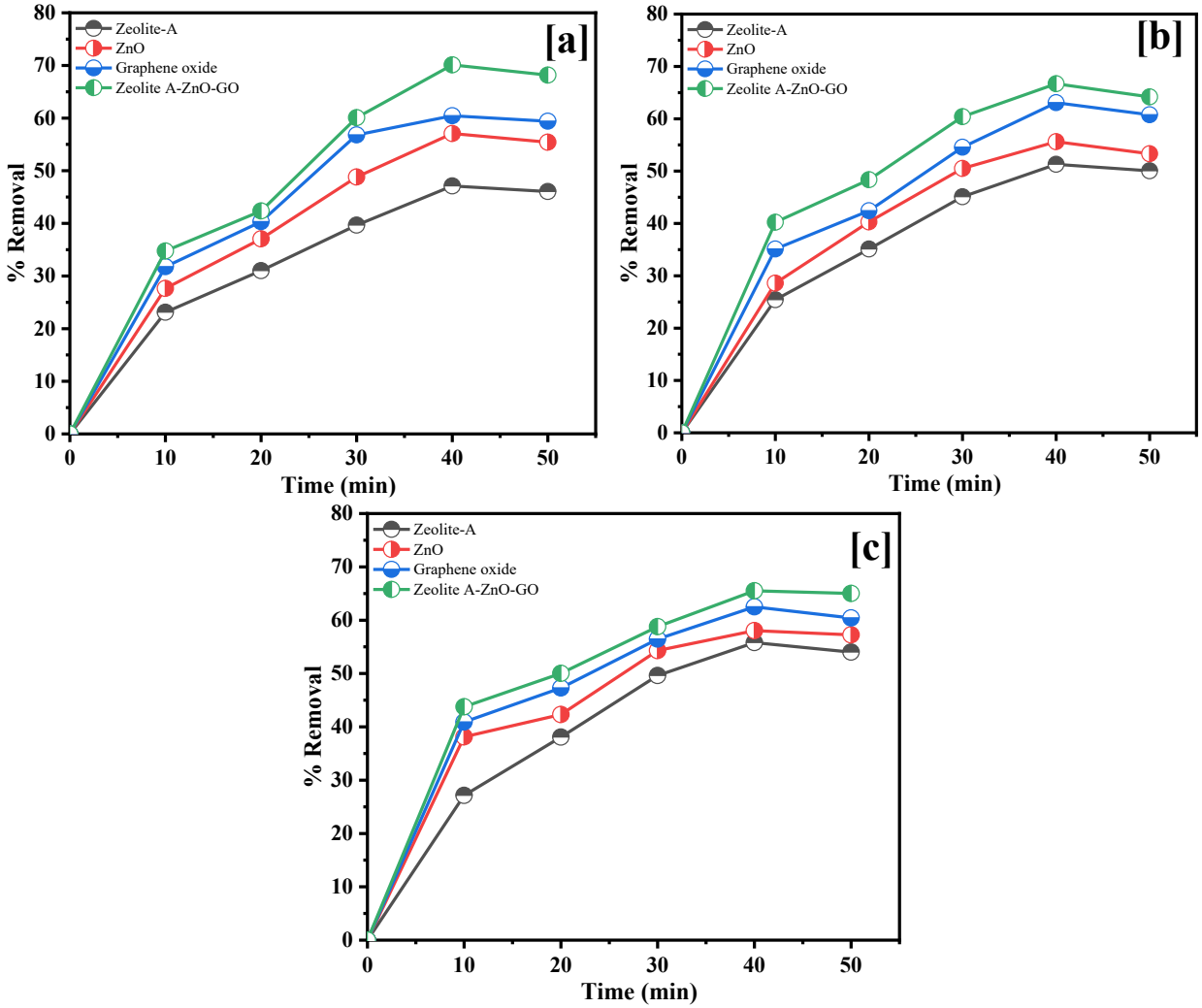


**Fig. 6: The contact times for the removal of (a) Cr (b) Fe and (c) Cd ions at pH = 4, dosage = 0.1 g and temperature = 25°C**

### 3.2.2 Dosage

The dosage of nanosorbents has a significant impact on the capacity of adsorption. Different dose concentrations, e.g., 0.3, 0.4, 0.5, 0.6, 0.7, and 0.8 g, were measured to investigate the efficiency removal process of Cd(II), Fe(II), and Cr(VI) by zeolite-A, ZnO, GO, and zeolite A -ZnO-GO hybrids in Fig. 7. Fig 7(a) depicts that raising the dosage increases the removal ability of Cd(II). The removal efficiencies at 0.3 g were 51.1%, 54.72%, 58.72%, and 65.1% for zeolite-A, ZnO, GO, and zeolite A-ZnO-GO, respectively. Increasing the dosage to 0.8 g, the removal efficiency increased significantly to 90.42%, 99.02%, and 100% for zeolite-A, ZnO, GO, and zeolite A-ZnO-GO, respectively. This increase is

explained by the availability of more binding sites on the surface of the nanosorbents, which promotes the adsorption of Cd(II). The maximum removal effectiveness was recorded for zeolite A-ZnO-GO because of its combined characteristics, resulting in a synergistic effect that promotes adsorption. Among the single nanosorbents, graphene oxide performed better than zeolite-A and ZnO because of its higher surface area (see Table 1) and functional groups for metal adsorption.

A similar trend was observed for the removal of Fe(II) ions, as depicted in Fig. 7(b). All these nanoparticles, in their lower dosages of 0.3 g, exhibited a removal efficiency of 53.8%, 59.04%, 67.72, and 72.06% by zeolite-A, ZnO, GO, and zeolite A-ZnO-GO, respectively. The increased dosage of 0.8 g resulted in 99.06% elimination efficiency for zeolite-A and 100% for other nanosorbents. Higher Fe(II) removal efficiency observed with the increasing dose of the nanosorbent is assigned to the fact that a higher dose provides more available surface area and binding sites for Fe(II) adsorption. Again, zeolite A-ZnO-GO showed higher adsorption capacity; it achieved complete removal at a lower dosage, namely 0.6 g. Fe(II) also manifested higher adsorption efficiency compared with Cd(II) under identical nanosorbent dosage, indicating higher intensification in the interaction between Fe(II) and the active sites of the nanosorbent.

Similarly, Cr(VI) adsorption increased with nanosorbent dosage, as depicted in Fig. 7(c). Correspondingly, at a dosage of 0.3 g, the removal efficiencies were 60.58% for zeolite-A, 65.51% for ZnO, 70.11% for GO, and 75.11% for zeolite A-ZnO-GO. Upon increasing the dosage to 0.8 g, all the nanosorbents recorded 100% elimination. The increased removal efficiency of Cr(VI), in comparison to Cd(II) and Fe(II), can be interpreted due to a smaller hydration radius and higher complexation affinity on the active site of nanosorbents. Complete removals of Cr(VI) were obtained at 0.6 g by GO and zeolite A-ZnO-GO, revealing the higher adsorption capacity for the formerly mentioned adsorbent. According to the selectivity sequence of the nanosorbents for the adsorption of metals, their order was observed as Cr(IV) > Fe(II) > Cd(II). This is probably because of the difference in ionic radii, hydration energy, and intensity of contact between the metal ions and nanosorbents (Uko *et al*. 2022). Cd(II) had the least removal efficiency at lower dosages, probably due to its larger hydrated radius of 0.404 nm and low electronegativity of 1.69. Thus, it has less affinity for the adsorption sites. In contrast, Fe(II) and Cr(VI) showed better adsorption with stronger interactions with nanosorbents.

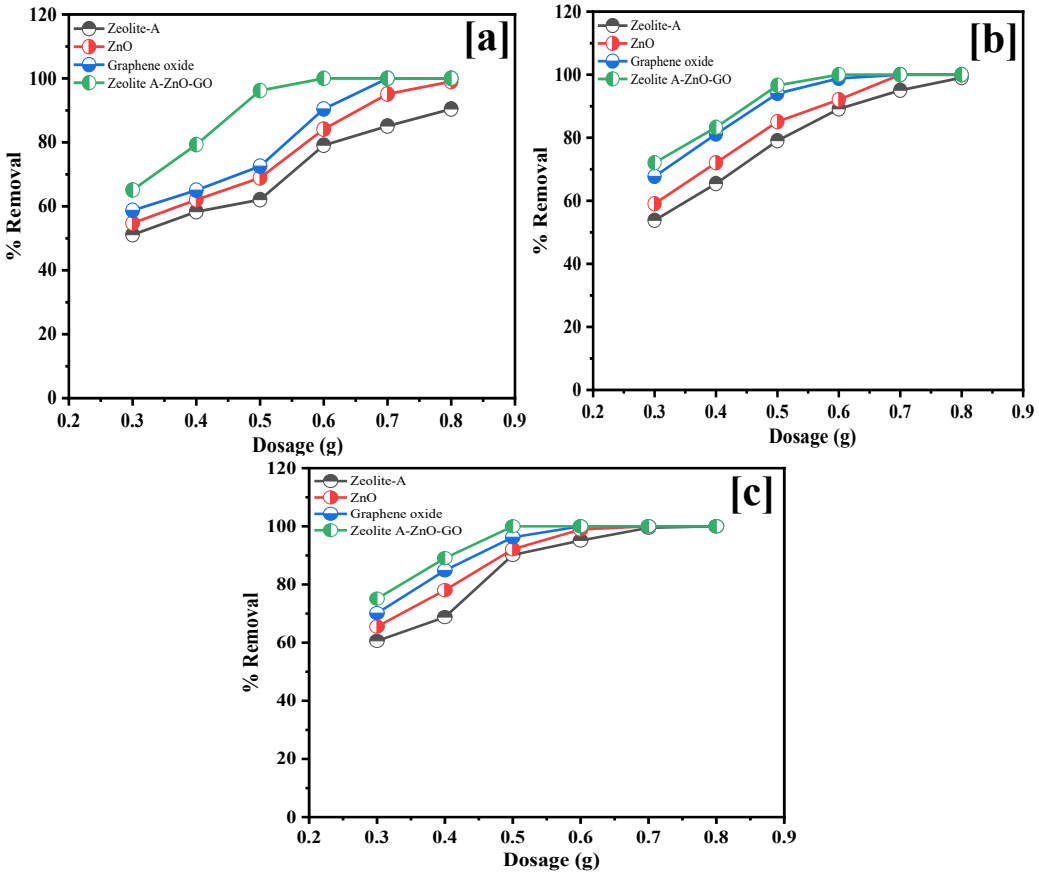


**Fig. 7: The effect of dosage for the removal of (a) Cd (b) Fe and (c) Cr ions at pH = 4, shaken at the optimum time, and temperature = 25°C**

### 3.2.3 Temperature

The influence of temperature on the removal of some heavy metals in wastewater is presented in Fig. 8. The removal efficiencies of Cd ions by zeolite-A, ZnO, GO, and zeolite A-ZnO-GO increased with temperature first (Fig. 8a). When the temperature rose to 30°C, their removal efficiencies reached 43.15%, 46.21%, 50.14%, and 55.61%, respectively. In addition, their removal efficiencies increased to 79.11%, 81.16%, 85.11%, and 90.11% with the increase in temperature to 70°C. This trend indicates that with the increase in temperature, there is a rise in adsorption capacity because of increased surface activity and more transportation of metal ions. However, the adsorption efficiency below 70°C can become constant due to the saturation of active sites and probable desorption effects.

Similar to Cd, Fe removal also increases with the increase in temperature (Fig. 8b). Corresponding temperature at 30°C, the removal efficiencies were 47.18%, 50.15%, 52.31%, and 58.5% for zeolite-A, ZnO, GO, and zeolite A-ZnO-GO, respectively. It kept on increasing with the rise in temperature and reached a maximum of 70°C with removal efficiencies of 82.02%, 82.25%, 88.07%, and 92.02%. With the rise in temperature, Fe ion mobility increased, hence increasing its contact possibility with the active adsorption sites. However, beyond 70°C, a plateau may be observed beyond which desorption takes over.

Cr ions showed the same adsorption trend, as illustrated in Fig. 8(c). At 30°C, their removal efficiencies were 52.41%, 52.25%, 55.07%, and 60.11% for zeolite-A, ZnO, GO, and zeolite A-ZnO-GO, respectively. By increasing the temperature, adsorption efficiencies increased and reached a maximum at 70°C: 86%, 83.5%, 89.46%, and 94.11%, respectively. The greater removal efficiency at higher temperatures is indicative of superior adsorption kinetics and higher contact rates between Cr ions and the adsorbent surface. At very high temperatures, however, the adsorption may stabilize or decrease due to probable desorption processes. The trend remains the same for all three metal ions: adsorption efficiency increases with temperature due to increased ion mobility and stronger contact with adsorbent surfaces. Among the adsorbents, zeolite A-ZnO-GO exhibited the highest removal efficiency, indicating its superior adsorption properties because of its composite structure. GO also outperformed ZnO and zeolite-A individually, probably due to its high surface area and active functional groups. The least adsorption was reported in zeolite-A, indicating it has fewer active sites for the removal of metal ions. With the rise in temperature, the adsorption of metal ions increased due to increased mobility, which allowed metal ions to gain energy and interact more effectively with the adsorbent surface (Mustapha *et al*. 2021). Beyond a certain temperature, the adsorption capacity of metal ions remained constant due to desorption, a process where metal ions started to detach from the adsorbent back into the solution.

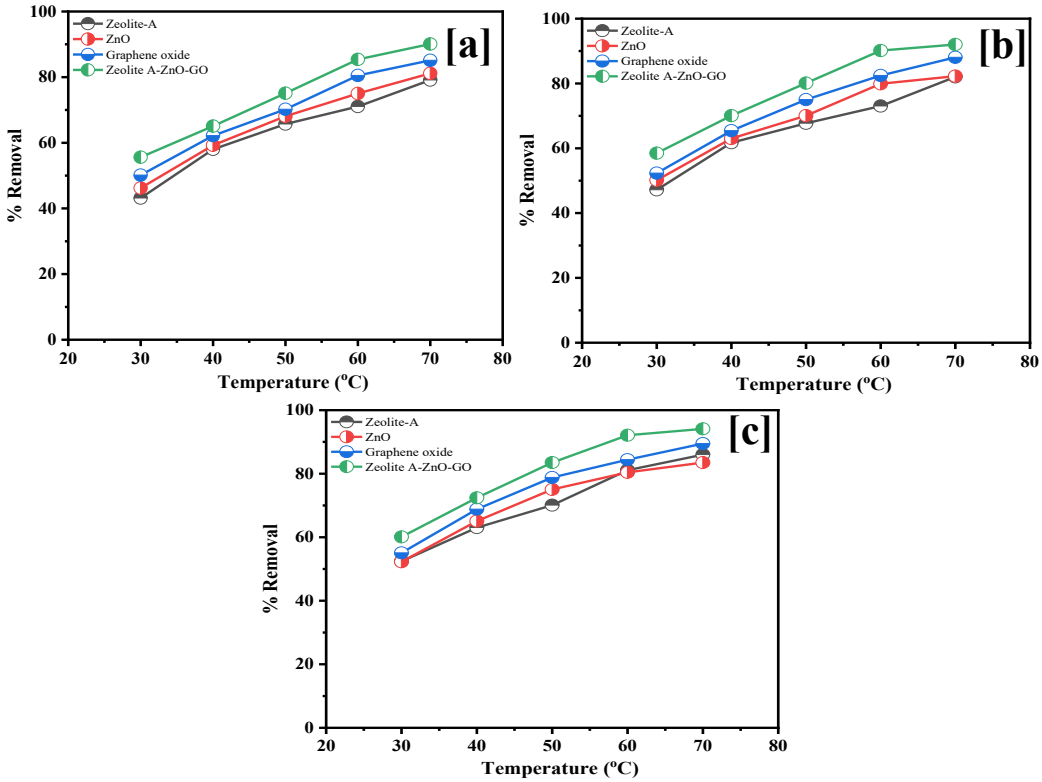


**Fig. 8: The effect of dosage for the removal of (a) Cd (b) Fe and (c) Cr ions at pH = 4, shaken at optimum time, and dosage = 0.1 g.**

### 3.3 Adsorption isotherms

The Langmuir isotherm model is used to describe the chemisorption and monolayer coverage of adsorbates onto adsorbents. Its linear form can be expressed by the following equation:

$$\frac{C_e}{q_e} = \frac{1}{K_L q_{max}} + \frac{C_e}{q_{max}} \quad (3)$$

where the amount of metal ions adsorbed at equilibrium in mg/g is $q_e$, the equilibrium concentration in mg/dm$^3$ is $C_e$, and the Langmuir constant ($K_L$) indicate the energy of adsorption.

The Freundlich isotherm model, which shows an exponential distribution of active sites and their energies and surface heterogeneity of the adsorbents, is described by the following equation:

$$\ln q_e = \frac{1}{n}\ln C_e + \ln K_f \quad (4)$$

where $K_f$ and n are the Freundlich constants related to the adsorption capacity and adsorption intensity, respectively. The values of $q_{max}$, $K_L$, $K_f$ and n obtained from both models are presented in Table 2. Where the maximum adsorption capacity values for Cr ions removal were as follows: zeolite A-ZnO-GO (107.92 mg/g), GO (106.01 mg/g), ZnO (99.34 mg/g), and zeolite A (92.42 mg/g). The $K_L$ values for all the adsorbents were below 1, which indicates that excellent adsorption has occurred. The correlation coefficient ($R^2$) values of the Langmuir model fall between 0.9912 to 0.9992, while that of Freundlich was in the range from 0.9476 to 0.9714, which infers that monolayer adsorption predominates. Further, for Cd ions, the order is zeolite A-ZnO-GO with the highest of 94.51 mg/g, followed by GO with 85.72 mg/g, ZnO with 81.56 mg/g, and zeolite A with 68.1 mg/g. $K_L$ values below 1 indicated good adsorption. The $R^2$ value for the Langmuir model, which was in the range of 0.9891-0.9954, was greater in comparison with that of Freundlich, ranging from 0.9385 to 0.9598, further indicating monolayer adsorption.

Quantitatively, zeolite A-ZnO-GO had a value of 98.28 mg/g for Fe ions, GO with 92.08 mg/g, ZnO with 83.17 mg/g, and zeolite A with an uptake of 79.54 mg/g. All the $K_L$ values were under 1, hence showing good adsorption. The Langmuir model fitted better from 0.9901 to 0.9989 than the Freundlich model from 0.939 to 0.9694, confirming monolayer adsorption. The experimental results obtained in this study fitted fairly well with both the Langmuir and Freundlich equations, fitting better into the Langmuir isotherm model. This suggests that the major adsorption process involves monolayer coverage of the adsorbents. Values of n greater than 1 indicate that the adsorption of Cr, Cd, and Fe ions onto the adsorbents is favorable. The maximum adsorption capacities estimated by the Langmuir model demonstrated that Zeolite A-ZnO-GO, compared with previous studies in Table 3, is the most efficient adsorbent in the removal of Cr, Cd, and Fe ions from wastewater.

**Table 2: Langmuir and Freudlich isotherm models parameters for the removal of Cr, Cd and Fe ions from wastewater**

| | | Freundlich | | | Langmuir | | |
|---|---|---|---|---|---|---|---|
| **Parameter** | **Sample** | **$K_f$** | **n** | **$R^2$** | **$q_{max}$** | **$K_L$** | **$R^2$** |
| Cr | Zeolite A | 12.16 | 2.06 | 0.9476 | 92.42 | 0.158 | 0.9912 |
| | ZnO | 15.78 | 1.86 | 0.9501 | 99.34 | 0.137 | 0.9962 |
| | GO | 23.04 | 1.76 | 0.966 | 106.01 | 0.096 | 0.9973 |
| | Zeolite A-ZnO-GO | 31.59 | 1.96 | 0.9714 | 107.92 | 0.084 | 0.9992 |
| Cd | Zeolite A | 10.54 | 2.14 | 0.9385 | 68.1 | 0.281 | 0.9891 |
| | ZnO | 13.02 | 1.85 | 0.947 | 81.56 | 0.209 | 0.9901 |
| | GO | 18.43 | 1.9 | 0.9507 | 85.72 | 0.19 | 0.992 |
| | Zeolite A-ZnO-GO | 22.81 | 1.72 | 0.9598 | 94.51 | 0.142 | 0.9954 |
| Fe | Zeolite A | 13.59 | 1.83 | 0.939 | 79.54 | 0.194 | 0.9901 |
| | ZnO | 14.64 | 2.18 | 0.9496 | 83.17 | 0.183 | 0.944 |
| | GO | 20.73 | 1.87 | 0.9638 | 92.08 | 0.136 | 0.9953 |
| | Zeolite A-ZnO-GO | 26.55 | 1.96 | 0.9694 | 98.28 | 0.129 | 0.9989 |

**Table 3: Comparison of maximum adsorption capacity with previous literature**

| **Material** | **Metal ion** | **Adsorption capacity (mg/g)** | **Reference** |
|---|---|---|---|
| Magnetic activated carbon | Cd | 73.3 | Zhang *et al*. (2021) |
| Magnetic composite material modified ion imprinting polymer (IIP@GO$Fe_3O_4$) | Cr | 8.502 | Neolaka *et al*. (2021) |
| Shanghai silty clay (SSC) | Cd | 2.80 | Wang and Zhang (2021) |
| | Cr | 1,85 | |
| Natural clay | Fe | 12.86 | Khalfa *et al*. (2021) |
| Acid activated clay | Fe | 19.25 | Khalfa *et al*. (2021) |
| Zeolite A-ZnO-GO | Cd | 94.51 | This study |

| | | | |
|---|---|---|---|
| Zeolite A-ZnO-GO | Fe | 98.28 | This study |
| Zeolite A-ZnO-GO | Cr | 106.01 | This study |

### 3.5 Adsorption kinetics

The adsorption kinetics was investigated using pseudo-first order and pseudo-second order models. The pseudo-first-order kinetic model is expressed by the following equation:

$$\ln(q_e - q_t) = \ln q_e - k_1 t \quad (5)$$

where $q_e$ and $q_t$ refer to the adsorption capacity of Cr, Cd, and Fe ions (mg/g) at equilibrium and at any time (min), respectively, and $k_1$ is the rate constant of pseudo-first-order adsorption (min). The pseudo-second-order kinetic rate equation is expressed as follows:

$$\frac{t}{q_t} = \frac{1}{k_2 q_e^2} + \frac{1}{q_e} t \quad (6)$$

where is $k_2$ the rate constant of pseudo-second order adsorption (g/mg min). The obtained parameters from pseudo-first-order and pseudo-second-order equations are listed in Table 4. It is observed that the correlation coefficient for the pseudo-first-order kinetic model in most cases is less than 92%, and thus, it resulted in a poor pseudo-first-order fitting to the experimental data. While the correlation coefficient for the pseudo-first-order adsorption model is too low, the values for the pseudo-second-order adsorption model are high, with most samples being more than 98%. Indeed, for Cr, Cd, and Fe ion removal, the pseudo-second-order kinetic model fits better. This suggests that the dominating mechanism is chemisorption and not physisorption. Values greater than 0.99 for the pseudo-second-order model, obtained for all materials in the present investigation, revealed that the mechanism of the adsorption process follows a chemical interaction mechanism involving electron exchange between the adsorbate and the adsorbent. The pseudo-second-order adsorption model has also been reported for various adsorbents such as $MgFe_2O_4$ nanoparticles (Nizam *et al*. 2024), alginate-clay (Aziam *et al*. 2024), activated carbon (Khalla *et al*. 2024), and P-type zeolite (Liu *et al*. 2024).

**Table 4: Kinetic models parameters for the removal of Cr, Cd and Fe ions from wastewater**

| | | 1st order | | | 2nd order | | |
|---|---|---|---|---|---|---|---|
| **Parameter** | **Sample** | $q_e$ | $k_1$ | $R^2$ | $q_e$ | $k_2$ | $R^2$ |
| Cr | Zeolite A | 20.06 | 0.162 | 0.9015 | 89.41 | 1.132 | 0.9907 |
| | ZnO | 31.74 | 0.201 | 0.917 | 93.59 | 1.351 | 0.9918 |
| | GO | 52.16 | 0.452 | 0.9245 | 100.18 | 2.912 | 0.9951 |
| | Zeolite A-ZnO-GO | 63.5 | 0.467 | 0.9311 | 109.5 | 3.051 | 0.999 |
| Cd | Zeolite A | 15.43 | 0.107 | 0.8982 | 65.55 | 1.016 | 0.9895 |
| | ZnO | 20.46 | 0.296 | 0.899 | 76.42 | 1.145 | 0.9902 |
| | GO | 29.08 | 0.315 | 0.9076 | 83.32 | 2.167 | 0.9914 |
| | Zeolite A-ZnO-GO | 35.11 | 0.327 | 0.9089 | 90.74 | 2.29 | 0.9921 |
| Fe | Zeolite A | 18.96 | 0.156 | 0.9007 | 75.3 | 1.108 | 0.9902 |
| | ZnO | 25.74 | 0.18 | 0.9142 | 80.68 | 1.272 | 0.991 |
| | GO | 48.03 | 0.381 | 0.9207 | 90.29 | 2.061 | 0.9946 |
| | Zeolite A-ZnO-GO | 51.84 | 0.409 | 0.9229 | 95.63 | 2.82 | 0.9988 |

### 3.5 Stability and reusability study

Fig. 9 presents the stability and reusability for zeolite-A, ZnO, graphene oxide, and zeolite A-ZnO-GO to realize practical applicability on Cr, Fe, and Cd remediation. From the five successive cycles obtained in the experiment, a fall in removal efficiencies could be achieved by all of these materials. Of these, the best stabilities and reusabilities upon interaction with the investigated metals corresponded to zeolite A-ZnO-GO in every case of the metals tested. The effective removal of Cr ions was tested using zeolite-A, ZnO, GO, and zeolite A-ZnO-GO over five cycles. From the results obtained, it is clear that most of the tested materials, in particular zeolite-A and ZnO, show a sharp decrease in their activities. The removal efficiency for Cr ions was 94.16% for zeolite-A, 98.6% for ZnO, 99% for GO, and 99.42% for zeolite A-ZnO-GO within the first cycle (Fig. 9a). In the fifth cycle, however, the removal efficiency significantly decreased to 64.52%, 78.81%, 83.45%, and 87.75%, respectively. The relatively higher removal efficiency of zeolite A-ZnO-GO in the fifth cycle may be explained by increased stability and reusability, possibly a synergistic effect of the composite structure that reduces its fast deactivation. For Fe ions (Fig. 9b), the removal efficiency was 90.45% for zeolite-A, 96.03% for ZnO, 99.61% for GO, and 98.8% for zeolite A-ZnO-GO during the first cycle. However, after five cycles, these further decreased to 62.51%, 76.51%, 80.15%, and 84.13%, respectively. Such a drastic loss in Fe removal by zeolite-A and ZnO shows that these materials are subjected to fast deactivation, probably by surface fouling or loss of active adsorption sites. Contrarily, the efficiency of the zeolite A-ZnO-GO composite remained reasonably high, which indicates that the combination of materials helps sustain structural integrity and prolongs its usability. The removal efficiencies of Cd ions in the first cycle for zeolite-A, ZnO, GO, and zeolite A-ZnO-GO were 92.17%, 95.14%, 96.03%, and 97.1%,

respectively (Fig. 9c). After five cycles, the removal efficiencies were reduced to 60.49%, 64.9%, 70.4%, and 79.65%, respectively. Noticeably, the most rapid efficiency reduction was that of ZnO, which suggested its poor stability in Cd removal. Among these, however, the zeolite A-ZnO-GO showed the best retention of efficiency, which could be indicative of improved reusability due to enhanced adsorption capacity and probable synergistic interactions among the components. Zeolite A-ZnO-GO consistently proved to be much more stable and reusable than the individual components, zeolite-A, ZnO, and GO, in the removal of Cr, Fe, and Cd ions. Efficiency decreased gradually to show that, indeed, all materials had suffered some level of degradation upon repeated use. However, the efficiency of zeolite A-ZnO-GO remains better, most likely due to improved adsorption, high surface area, reduced surface fouling, and increased structural stability. Based on these observations, zeolite A-ZnO-GO can be considered a prospective material for real applications concerning heavy metal remediation.

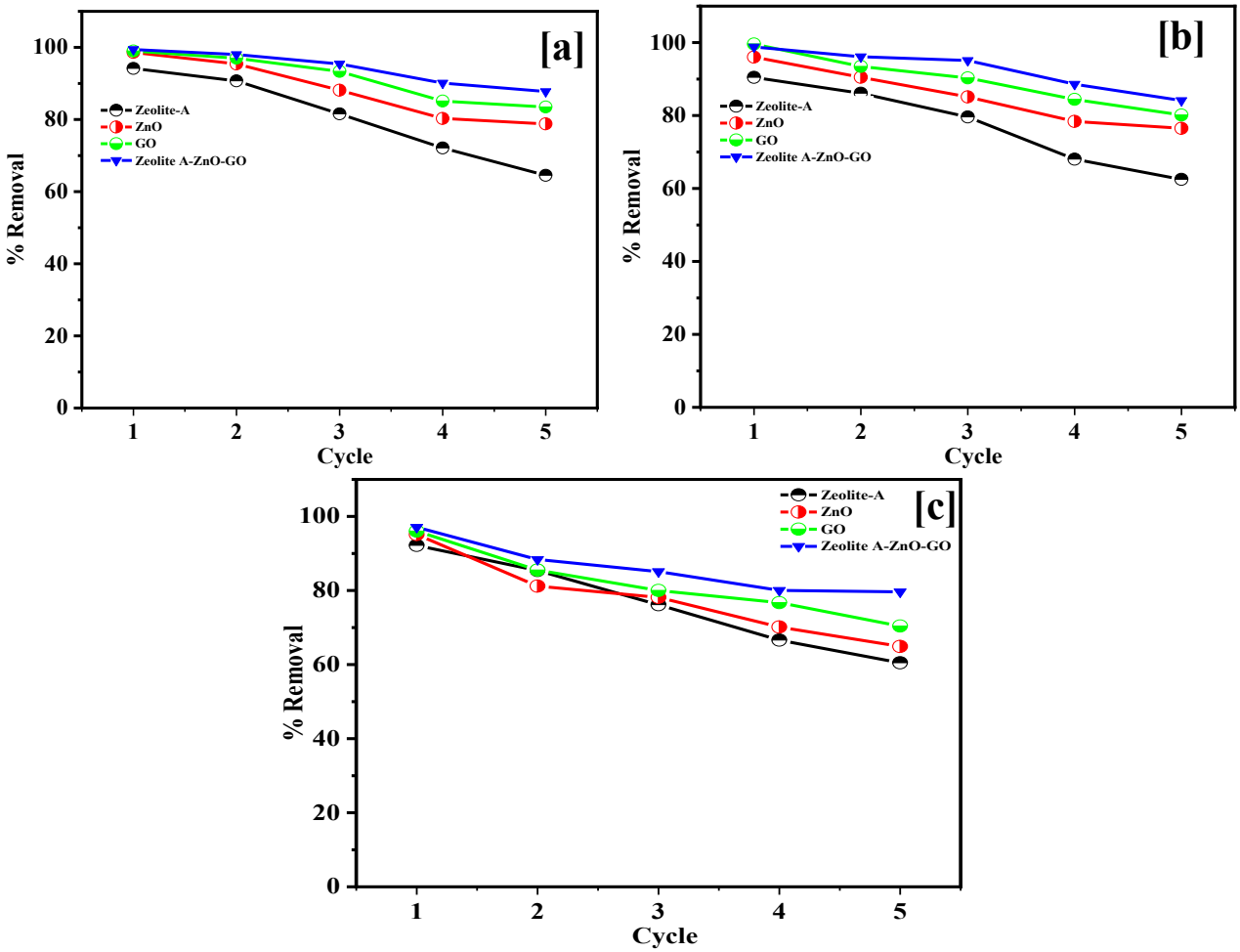


**Fig. 9: The recyclability of the spent adsorbent for the removal of (a) Cr (b) Fe and (c) Cd ions**

## 4. CONCLUSION

The adsorption studies showed that the composite outperformed its constituents in removing Cd(II), Fe(II), and Cr(VI) ions from pharmaceutical effluent: the removal efficiencies attained equilibrium within 40–50 min. The composite attained maximum removal rates of 70.11% for Cr, 66.7% for Fe, and 65.51% for Cd. As the adsorbent dose was increased, the removal efficiency also increased, with 100% elimination at 0.8 g for the three metals. Temperature studies revealed that up to 70°C, adsorption capacity increased with the rise in temperature, indicating that it was endothermic in nature and increased the interaction between metal ions and the adsorbent surface. Modeling of isotherm revealed that adsorption follows the Langmuir model, indicating monolayer adsorption and kinetic studies indicated that adsorption follows a pseudo-second-order model, thus indicating chemisorption as the major mechanism. It demonstrated great stability and reusability, maintaining high removal efficiencies over cycles, hence revealing its practical viability in heavy metal remediation from wastewater treatment. Zeolite-A/ZnO/GO nanocomposites have proven to be highly effective, stable, and reusable adsorbents in heavy metal removal. Its surface area has expanded, and more effective adsorption sites with synergetic interaction turn it appropriate for environmental applications.

**Competing interests:** The authors declared no conflict of interest and no known competing financial interests.

**Credit authorship contribution statement**

**Conceptualization, planning, and writing**: Ibrahim Salihu Zungeru, Muhammad Aliyu, Binta Saidu, Amos Ndarubu Tsado and Amos Ndarubu Tsado.

**Review writing**: John Tsado Mathew, Olusayo Oyeronke Kolo, Rakiya Zubairu, and Saheed Mustapha. All authors read and approved the final manuscript.

**Acknowledgments**

In appreciation for funding this study, the authors are grateful to the Tertiary Education Trust Fund (TET Fund) and the management of Niger state polytechnic Zungeru for fostering an enabling research environment

## REFERENCES


- Abou Zeid, S., & Leprince-Wang, Y. (2024). Advancements in ZnO-based photocatalysts for water treatment: a comprehensive review. *Crystals*, *14*(7), 611.
- Al-Abbad, E. A., & Al Dwairi, R. A. (2021). Removal of nickel (II) ions from water by Jordan natural zeolite as sorbent material. *Journal of Saudi chemical society*, *25*(5), 101233.
- Bakhtiari, S., Salari, M., Shahrashoub, M., Zeidabadinejad, A., Sharma, G., & Sillanpää, M. (2024). A Comprehensive Review on Green and Eco-Friendly Nano-Adsorbents for the Removal of Heavy Metal Ions: Synthesis, Adsorption Mechanisms, and Applications. *Current Pollution Reports*, *10*(1), 1-39.
- Benalia, M. C., Youcef, L., Bouaziz, M. G., Achour, S., & Menasra, H. (2022). Removal of heavy metals from industrial wastewater by chemical precipitation: mechanisms and sludge characterization. *Arabian Journal for Science and Engineering*, *47*(5), 5587-5599.
- Elsamra, R. M., Masoud, M. S., Zidan, A. A., Zokm, G. M. E., & Okbah, M. A. (2024). Green synthesis of nanostructured zinc oxide by Ocimum tenuiflorum extract: characterization, adsorption modeling, cytotoxic screening, and metal ions adsorption applications. *Biomass Conversion and Biorefinery*, *14*(15), 16843-16856.
- Eren, S., Türk, F. N., & Arslanoğlu, H. (2024). Synthesis of zeolite from industrial wastes: a review on characterization and heavy metal and dye removal. *Environmental Science and Pollution Research*, 1-33.
- Etsuyankpa, M. B., Augustine, A. U., Musa, S. T., Mathew, J. T., Ismail, H., Salihu, A. M., Mamman, A (2024). An Overview of Wastewater Characteristics, Treatment and Disposal: A Review. *Journal of Applied Science and Environmental Management,* 28 (5) 1553-1572.
- Gopalakrishnan, A., Krishnan, R., Thangavel, S., Venugopal, G., & Kim, S. J. (2015). Removal of heavy metal ions from pharma-effluents using graphene-oxide nanosorbents and study of their adsorption kinetics. *Journal of Industrial and Engineering Chemistry*, *30*, 14-19.
- Guida, S., Rubertelli, G., Jefferson, B., & Soares, A. (2021). Demonstration of ion exchange technology for phosphorus removal and recovery from municipal wastewater. *Chemical Engineering Journal*, *420*, 129913.
- Hu, L., Yan, G., Chauhan, B. S., Elbadawy, I., Abouelela, M., Marefati, M., & Salah, B. (2023). Development and evaluation of an electro-Fenton-based integrated hydrogen production and wastewater treatment plant coupled with the solar and electrodialysis units. *Process Safety and Environmental Protection*, *177*, 568-580.
- Khalfa, L., Cervera, M. L., Souissi-Najjar, S., & Bagane, M. (2021). Removal of Fe (III) from synthetic wastewater into raw and modified clay: Experiments and models fitting. *Separation Science and Technology*, *56*(4), 708-718.
- Khalla, D., Belguidoum, K., Nacef, M., Boukour, M., Chelaghmia, M.L., Khelifi, O., Selaimia, R., Bengourna, N., Affoune, A.M. and Amira-Guebailia, H., 2024. Competitive adsorption of quinary heavy metal ions onto chestnut shell activated carbon. *Materials Chemistry and Physics*, *323*, p.129646.
- Liu, Z., & Cheng, X. (2024). Preparation and characterization of P-type zeolite for adsorption of Cr3+, Ni2+, and Co2+. *Environmental Science and Pollution Research*, *31*(16), 23664-23679.
- Mathew, J. T., Musah, M., Azeh, Y. and Musa, M. (2024)a. Removal of Some Toxic Metals from Pharmaceutical Wastewater Using Geopolymer/$Fe_3O4$/ZnO nanocomposite: Isotherm, Kinetics and Thermodynamic Studies. Confluence University Journal of Science and Technology, 1(1): 50-58.
- Mathew, J. T., Musah, M., Azeh, Y. & Muhammed, M. (2024)b. Development of Fe3O4 Nanoparticles for the Removal of Some Toxic Metals from Pharmaceutical Wastewater. Caliphate Journal of Science & Technology (CaJoST), 6(1), 26-34.
- Mathew, J. T., Musah, M., Azeh, Y. & Muhammed, M. (2023)a. Adsorptive Removal of Selected Toxic Metals from Pharmaceutical Wastewater using $Fe_3O_4$/ZnO Nanocomposite, *Dutse Journal of Pure and Applied Sciences*, 9(4a), 236- 248
- Mathew, J. T., Musah, M., Azeh, Y. & Muhammed, M. (2023)b. Kinetic Study of Heavy Metals Removal from Pharmaceutical Wastewater Using Geopolymer/$Fe_3O_4$ Nanocomposite. Bima Journal of Science and Technology, 7(4), 152- 163.
- Musa A. V., Musah, M. and Mathew, J. T. (2024). Production and characterization of Zeolite-A nanoparticles for the treatment of pharmaceutical

wastewater. *Science World Journal Vol.* 19(4), 987-993.

- Mustapha, S., Tijani, J. O., Ndamitso, M. M., Abdulkareem, A. S., Shuaib, D. T., & Mohammed, A. K. (2021). Adsorptive removal of pollutants from industrial wastewater using mesoporous kaolin and kaolin/TiO2 nanoadsorbents. *Environmental Nanotechnology, Monitoring & Management*, *15*, 100414.
- Neolaka, Y.A., Lawa, Y., Naat, J., Riwu, A.A., Lindu, Y.E., Darmokoesoemo, H., Widyaningrum, B.A., Iqbal, M. and Kusuma, H.S., 2021. Evaluation of magnetic material IIP@ GO-Fe3O4 based on Kesambi wood (Schleichera oleosa) as a potential adsorbent for the removal of Cr (VI) from aqueous solutions. *Reactive and Functional Polymers*, *166*, p.105000.
- Nizam, T., Krishnan, K. A., Joseph, A., & Krishnan, R. R. (2024). Isotherm, kinetic and thermodynamic modelling of liquid phase adsorption of the heavy metal ions Zn (II), Pb (II) and Cr (VI) onto MgFe2O4 nanoparticles. *Groundwater for Sustainable Development*, *25*, 101120.
- Ponnusami, A.B., Sinha, S., Ashokan, H., Paul, M.V., Hariharan, S.P., Arun, J., Gopinath, K.P., Le, Q.H. and Pugazhendhi, A., 2023. Advanced oxidation process (AOP) combined biological process for wastewater treatment: A review on advancements, feasibility and practicability of combined techniques. *Environmental research*, *237*, p.116944.
- Rahman, Z., & Singh, V. P. (2019). The relative impact of toxic heavy metals (THMs)(arsenic (As), cadmium (Cd), chromium (Cr)(VI), mercury (Hg), and lead (Pb)) on the total environment: an overview. *Environmental monitoring and assessment*, *191*, 1-21.
- Raj, S., Singh, H., & Bhattacharya, J. (2023). Treatment of textile industry wastewater based on coagulation-flocculation aided sedimentation followed by adsorption: Process studies in an industrial ecology concept. *Science of The Total Environment*, *857*, 159464.
- Razzak, S.A., Faruque, M.O., Alsheikh, Z., Alsheikhmohamad, L., Alkuroud, D., Alfayez, A., Hossain, S.Z. and Hossain, M.M., 2022. A comprehensive review on conventional and biological-driven heavy metals removal from industrial wastewater. *Environmental Advances*, *7*, p.100168.
- Shaba, E. Y., Tijani, J. O., Jacob, J. O., Suleiman, M. A.T. & Mathew, J. T. (2024). Preparation, characterization, adsorptive and antimicrobial properties of $Fe_3O_4$@$SiO_2$@ZnO nanocomposite. Colloids and Surfaces A: Physicochemical and Engineering Aspects, 686, 1-17.
- Uko, C. A., Tijani, J. O., Abdulkareem, S. A., Mustapha, S., Egbosiuba, T. C., & Muzenda, E. (2022). Adsorptive properties of MgO/WO3 nanoadsorbent for selected heavy metals removal from indigenous dyeing wastewater. *Process safety and environmental protection*, *162*, 775-794.
- Wang, J., & Zhang, W. (2021). Evaluating the adsorption of Shanghai silty clay to Cd (II), Pb (II), As (V), and Cr (VI): Kinetic, equilibrium, and thermodynamic studies. *Environmental monitoring and assessment*, *193*(3), 131.
- Zahmatkesh, S., Karimian, M., Chen, Z., & Ni, B. J. (2024). Combination of coagulation and adsorption technologies for advanced wastewater treatment for potable water reuse: By ANN, NSGA-II, and RSM. *Journal of Environmental Management*, *349*, 119429.
- Zhang, Z., Wang, T., Zhang, H., Liu, Y., & Xing, B. (2021). Adsorption of Pb (II) and Cd (II) by magnetic activated carbon and its mechanism. *Science of the Total Environment*, *757*, 143910.